Accurate waveforms for non-spinning binary black holes using the effective-one-body approach

Alessandra Buonanno,[1] Yi Pan,[1] John G. Baker,[2] Joan Centrella,[2]
Bernard J. Kelly,[2] Sean T. McWilliams,[3] and James R. van Meter[2,4]

[1]*Maryland Center for Fundamental Physics*
Department of Physics, University of Maryland, College Park, MD 20742
[2]*Gravitational Astrophysics Laboratory, NASA Goddard Space Flight Center, 8800 Greenbelt Rd., Greenbelt, MD 20771*
[3]*Department of Physics, University of Maryland, College Park, MD 20742*
[4]*Center for Space Science & Technology, University of Maryland Baltimore County,*
Physics Department, 1000 Hilltop Circle, Baltimore, MD 21250

(Dated: June 7, 2007)

Using numerical relativity as guidance and the natural flexibility of the effective-one-body (EOB) model, we extend the latter so that it can successfully match the numerical relativity waveforms of non-spinning binary black holes during the last stages of inspiral, merger and ringdown. Here, by successfully, we mean with phase differences $\lesssim 8\%$ of a gravitational-wave cycle accumulated until the end of the ringdown phase. We obtain this result by simply adding a 4 post-Newtonian order correction in the EOB radial potential and determining the (constant) coefficient by imposing high-matching performances with numerical waveforms of mass ratios $m_1/m_2 = 1, 2/3, 1/2$ and $= 1/4$, m_1 and m_2 being the individual black-hole masses. The final black-hole mass and spin predicted by the numerical simulations are used to determine the ringdown frequency and decay time of three quasi-normal-mode damped sinusoids that are attached to the EOB inspiral-(plunge) waveform at the light-ring. The accurate EOB waveforms may be employed for coherent searchs of gravitational waves emitted by non-spinning coalescing binary black holes with ground-based laser-interferometer detectors.

PACS numbers:

I. INTRODUCTION

The network of ground-based laser-interferometer gravitational-wave (GW) detectors, such as LIGO [1], VIRGO [4], GEO [2] and TAMA [3], are currently operating at design sensitivity (except for VIRGO which plans to reach design sensitivity within one year) and are searching for GWs in the frequency range of 10–10^3 Hz. Within the next decade those detectors will likely be complemented by the laser-interferometer space antenna (LISA) [5], a joint venture between NASA and ESA, which will search for GWs in the frequency range 5×10^{-5}–10^{-2} Hz.

Binary systems composed of black holes (BHs) and/or neutron stars (NSs) are among the most promising sources. The search for GWs from coalescing binary systems and the extraction of parameters are based on the matched-filtering technique [6], which requires accurate knowledge of the waveform of the incoming signal. Recent comparisons [8–11] between numerical and post-Newtonian (PN) analytic waveforms emitted by non-spinning binary BH systems suggest that it should be possible to design purely analytic templates with the full numerics used to guide the patching together of the inspiral and ringdown waveforms. This is an important avenue to template construction as eventually thousands of waveform templates may be needed to extract the GW signal from the noise, an impossible demand for numerical relativity (NR) alone.

The best-developed *analytic* method for describing the two-body dynamics of comparable-mass BHs and predicting the GW signal is undoubtedly the PN method [7], which for compact bodies is essentially an expansion in the characteristic orbital velocity v/c. Predictions are currently available through 3.5PN order [14–17] (v^7/c^7), if the compact objects do not carry spin, and 2.5PN order [18] (v^5/c^5) if they carry spin. Resummation of the PN expansion aimed at pushing analytic calculations until the final stage of evolution, including the transition inspiral–merger–ringdown, have been proposed. In 1999, the authors of Ref. [21] introduced a non-perturbative resummation of the two-body conservative dynamics, the so-called effective-one-body (EOB) approach [21]. The original EOB model was computed using the 2PN conservative dynamics. It was then extended to 3PN order [23] when the 3PN calculation was completed [17] and then to spinning BHs [24]. The EOB approach has been the *only* analytic approach able to predict, within $\sim 10\%$ of accuracy, the spin and mass of the final BH [25], and to provide a complete waveform, from inspiral to ringdown, for non-spinning [25, 26] and spinning, precessing binary systems [27]. To include accurately the radiation-reaction contribution, the EOB approach uses the Padé resummation of the GW flux, as proposed in Ref. [28].

As we shall see below, because of the reduction of the dynamics to *a few* crucial functions determining the inspiral evolution, and because of the rather simple procedure to match the inspiral(-plunge) waveform to the ringdown waveform, the EOB model is particularly suitable for fitting to the numerical results [12, 13]. In this paper we shall employ its flexibility to obtain accurate

waveforms for non-spinning binary BHs with mass ratios ranging between $m_1/m_2 = 1$ and $m_1/m_2 = 1/4$, with m_1 and m_2 being the BH masses. The method also allows us to predict the waveforms for mass ratios $m_1/m_2 < 1/4$. Those waveforms will be tested against numerical results when accurate long numerical simulations for mass ratios $m_1/m_2 < 1/4$ become available. In this paper the comparisons are carried out using simulations from the NASA-Goddard group.

The paper is organized as follows. In Sec. II we briefly review the EOB model. In Sec. III we *improve* the EOB model by adding a 4PN order unknown coefficient to the two-body conservative dynamics. In Sec. IV we compare this improved EOB model to two accurate, long numerical simulations having mass ratios 1 : 1 and 1 : 4, determine the best-fit 4PN order coefficient and discuss the matching performances. Section V summarizes our main conclusions. In Appendix A we extend the comparison to several multipole moments, and in Appendix B to shorter numerical simulations having mass ratios 1 : 2 and 2 : 3.

II. THE EFFECTIVE-ONE-BODY MODEL

The resummation technique discussed in this section, the EOB approach [21], was originally inspired by a similar approach introduced by Brézin, Itzykson and Zinn-Justin [22] to study two electromagnetically interacting particles having comparable masses. The basic idea of the EOB approach is to map the *real* conservative two-body dynamics up to the highest PN order available, onto an *effective* one-body problem, where a test particle of mass $\mu = m_1 m_2/M$, with m_1, m_2 the black-hole masses and $M = m_1 + m_2$, moves in some effective background metric $g^{\rm eff}_{\mu\nu}$. This mapping has been worked out within the Hamilton-Jacobi formalism, by imposing that whereas the action variables of the real and effective description coincide, i.e. $L_{\rm real} = L_{\rm eff}$, $\mathcal{I}_{\rm real} = \mathcal{I}_{\rm eff}$, where L denotes the total angular momentum, and $\mathcal{I}$ the radial action variable, the energy axis is allowed to change, $E_{\rm real} = f(E_{\rm eff})$, where f is a generic function determined by the mapping. By applying the above rules defining the mapping, it was found [21] that as long as radiation-reaction effects are not taken into account, the effective metric is just a deformation of the Schwarzschild metric, with deformation parameter $\eta = \mu/M$.

The explicit expression of the non-spinning EOB effective Hamiltonian through 3PN order is [21, 23]:

$$H_{\rm eff}(\mathbf{r},\boldsymbol{p}) = \mu\,\widehat{H}_{\rm eff}(\mathbf{r},\mathbf{p}) = \mu\sqrt{A(r)\left[1+\mathbf{p}^2+\left(\frac{A(r)}{D(r)}-1\right)(\mathbf{n}\cdot\mathbf{p})^2+\frac{1}{r^2}\left(z_1(\mathbf{p}^2)^2+z_2\,\mathbf{p}^2(\mathbf{n}\cdot\mathbf{p})^2+z_3(\mathbf{n}\cdot\mathbf{p})^4\right)\right]}\,, \quad (1)$$

with $\mathbf{r}$ and $\mathbf{p}$ being the reduced dimensionless variables; $\mathbf{n} = \mathbf{r}/r$ where we set $r = |\mathbf{r}|$. In absence of spins the motion is constrained to a plane. Introducing polar coordinates $(r, \varphi, p_r, p_\varphi)$, the EOB effective metric reads

$$ds^2_{\rm eff} \equiv g^{\rm eff}_{\mu\nu}\,dx^\mu\,dx^\nu = -A(r)\,c^2dt^2 + \frac{D(r)}{A(r)}\,dr^2 + r^2\left(d\theta^2+\sin^2\theta\,d\varphi^2\right). \quad (2)$$

The EOB real Hamiltonian is

$$H_{\rm real} = M\,\hat{H}_{\rm real} = M\sqrt{1+2\eta\left(\frac{H_{\rm eff}-\mu}{\mu}\right)} - M\,, \quad (3)$$

Remarkably, as originally observed in Ref. [21], the mapping between the real and the effective Hamiltonians given by Eq. (3) coincides with the mapping obtained in the context of quantum electrodynamics in Ref. [22], where the authors mapped the one-body relativistic Balmer formula onto the two-body energy formula. Moreover, Eq. (3) holds at 2PN and 3PN order [23]. The coefficients z_1, z_2 and z_3 in Eq. (1) are arbitrary, but subject to the constraint

$$8z_1 + 4z_2 + 3z_3 = 6(4-3\eta)\,\eta\,. \quad (4)$$

The coefficients $A(r)$ and $D(r)$ in Eq. (1) have been calculated through 3PN order [21, 23]. In the Taylor-expanded form they read:

$$A^{\rm 3PN}_T(r) = 1 - \frac{2}{r} + \frac{2\eta}{r^3} + \left[\left(\frac{94}{3}-\frac{41}{32}\pi^2\right)\eta - z_1\right]\frac{1}{r^4}\,, \quad (5)$$

$$D^{\rm 3PN}_T(r) = 1 - \frac{6\eta}{r^2} + \left[7z_1 + z_2 + 2\eta\,(3\eta-26)\right]\frac{1}{r^3}\,. \quad (6)$$

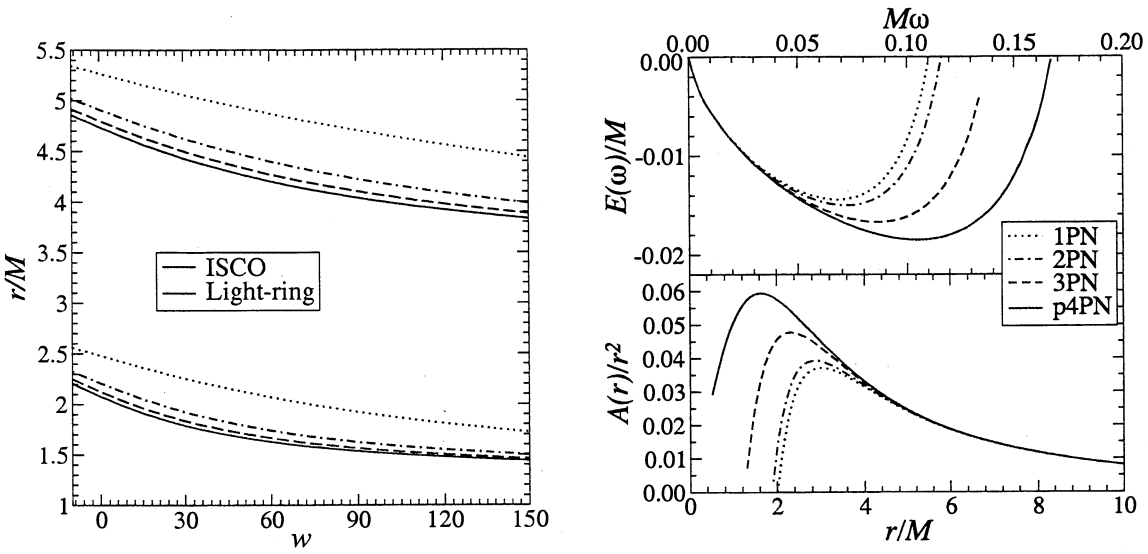

FIG. 1: In the left panel we show the position of the ISCO and light-ring as function of the parameter w, for different mass ratios. In the right panel we show the energy for circular orbits as a function of the frequency evaluated from the EOB Hamiltonian and the radial potential as a function of the radial coordinate for a massless particle in the EOB model. The various curves refer to different PN orders.

In principle we could explore the possibility of determining some of the z_i coefficients through a fit with the numerical results. However, here we do not follow this possibility and, as in previous works, set $z_1 = z_2 = 0$, thus $z_3 = 2(4-3\eta)\eta$. The EOB effective potential $A_T^{\rm 3PN}(r)$ does not lead to a last-stable circular orbit (LSO), contrary to what happens in the 2PN-accurate case [21]. This is due to the rather large value of the 3PN coefficient $94/3 - 41/32\pi^2 \simeq 18.688$ entering the PN expansion of $A(r)$. Replacing the PN-expanded form of $A(r)$ by a Padé approximant cures this problem [23]. The Padé approximant is

$$A_{P_2^1}^{\rm 2PN}(r) = \frac{r\,(-4+2r+\eta)}{2r^2+2\eta+r\,\eta}\,, \tag{7}$$

at 2PN order and

$$A_{P_3^1}^{\rm 3PN}(r) = \frac{r^2\left[(a_4(\eta,0)+8\eta-16)+r\,(8-2\eta)\right]}{r^3\,(8-2\eta)+r^2\left[a_4(\eta,0)+4\eta\right]+r\left[2a_4(\eta,0)+8\eta\right]+4[\eta^2+a_4(\eta,0)]}\,, \tag{8}$$

at 3PN order where

$$a_4(\eta,\tilde{z}_1) = \left[\eta\left(\frac{94}{3}-\frac{41}{32}\pi^2\right)-z_1\right]. \tag{9}$$

To include radiation-reaction effects we write the EOB Hamilton equations in terms of the reduced quantities $\widehat{H}$ and $\widehat{t} = t/M$, $\widehat{\omega} = \omega\, M$ [25], as [54]

$$\frac{dr}{d\widehat{t}} = \frac{\partial\widehat{H}}{\partial p_r}(r,p_r,p_\varphi)\,, \tag{10}$$

$$\frac{d\varphi}{d\widehat{t}} \equiv \widehat{\omega} = \frac{\partial\widehat{H}}{\partial p_\varphi}(r,p_r,p_\varphi)\,, \tag{11}$$

$$\frac{dp_r}{dt} = -\frac{\partial\widehat{H}}{\partial r}(r,p_r,p_\varphi)\,, \tag{12}$$

$$\frac{dp_\varphi}{d\widehat{t}} = \widehat{F}^\varphi[\widehat{\omega}(r,p_r,p_\varphi)]\,, \tag{13}$$

where for the φ component of the radiation-reaction force

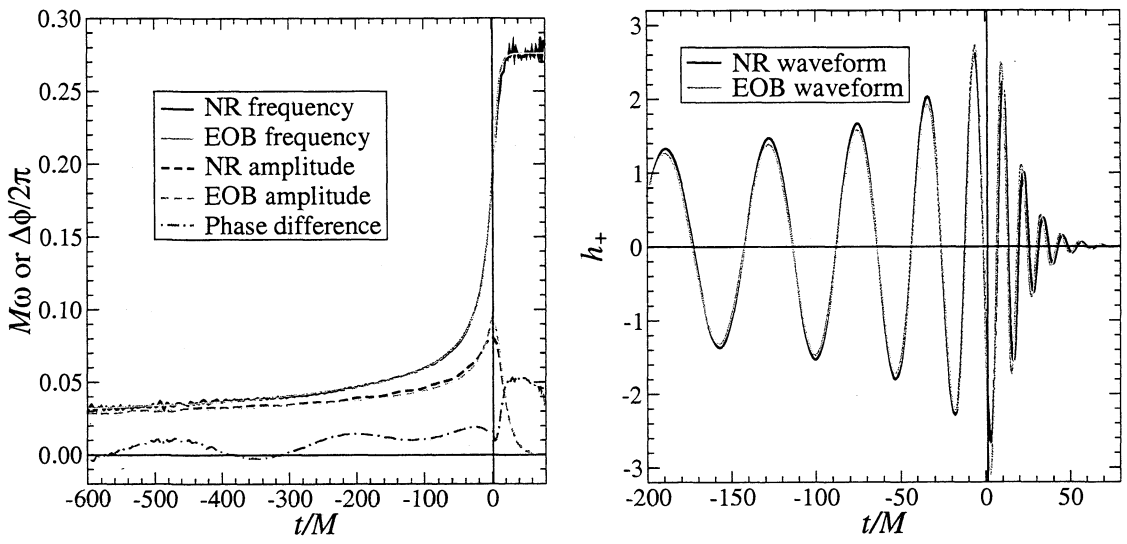

FIG. 2: Equal-mass binary. In the left panel we plot the NR and EOB frequencies and amplitudes, and the phase difference between the EOB and NR h_{22}. In the right panel we compare the EOB and NR h_{22} extracted perpendicularly to the orbital plane. We maximize only on the initial phase and time of arrival.

we shall the P-approximant [25, 28]

$$\widehat{F}^{\varphi}_{P_N} \equiv -\frac{1}{\eta\, v_\omega^3}\,\mathcal{F}_{P_N}[v_\omega] = -\frac{32}{5}\,\eta\, v_\omega^7\,\frac{f_{P_N}(v_\omega;\eta)}{1-v_\omega/v_{\rm pole}(\eta)}\,, \tag{14}$$

where $v_\omega \equiv \widehat{\omega}^{1/3} \equiv (d\varphi/d\widehat{t})^{1/3}$. The coefficients f_{P_N} can be read from Eqs. (XXX) in Ref. [42], while we set $v_{\rm pole} = 1$. In Refs. [44], the authors pointed out that a more accurate expression of the radiation-reaction force should not use the Keplerian relation between r and ω when the binary evolves inside the LSO. We find that this modification has a negligible effect on the waveform.

The last crucial ingredient of the EOB model is the inclusion of the ringdown phase. After the two BHs merge, the system settles down to a Kerr BH and emits quasi-normal modes (QNMs) [49, 50]. In the test-mass limit, $\eta \ll 1$, Refs. [50, 51] realized that when a test particle falls radially below $3M$ (the unstable light-ring of Schwarzschild), it immediately triggers the production of QNMs. In the equal-mass case $\eta = 1/4$, Ref. [52] proposed the so-called close-limit approximation, which consists in switching from the two-body description to the one-body description (perturbed-BH) close to the light-ring location. Based on these observations, Ref. [21] modeled the merger as a very short (instantaneous) phase and matched the inspiral(-plunge) waveform at the light-ring to a damped sinusoid. The frequency and decay time were computed estimating the final BH mass and spin from the EOB energy and angular momentum at the matching point. The matching procedure has then been improved, by adding more QNMs, extending it to several multipole moments [8, 53], and applying it in an time-interval instead of one point in time [46].

III. IMPROVING THE EFFECTIVE-ONE-BODY MODEL

Previous investigations [8, 10] focusing on comparable mass binaries, have shown that a non-negligible dephasing can accumulate at the transition inspiral(-plunge) to ringdown between the EOB waveform, computed through 3.5 PN order, and the NR waveform. The dephasing is caused by the much fast increase of the GW frequency in the 3.5PN-EOB model than in the NR simulation. Although the dephasing will prevent to accurately determine the binary parameters, it will not prevent to detect the waveform. In Ref. [10] the EOB matching to ringdown employed three extra parameters describing the time of matching, and the difference between the final BH mass (spin) and the energy (angular-momentum) at the point of matching. In this paper we shall improve the matching getting rid of the three extra parameters and reducing the dephasing to $\lesssim 0.08$ of a GW cycles, thus providing accurate waveforms depending *only* on the BH masses to be used for coherent detection and parameter estimation.

To decrease the differences between the EOB and NR waveforms during the last stages of inspiral and plunge, we introduce a 4PN order term in the effective potential $A(r)$ and Padé approximate it using the approximant $A^{P^1_4}$. Similar modifications were employed in Ref. [33] to obtain better matches of the EOB model to quasi-equilibrium initial-data configurations [34]. Since the 4PN term has not been calculated in PN theory, we shall denote it as "p4PN", where "p" stands for *pseudo*. We

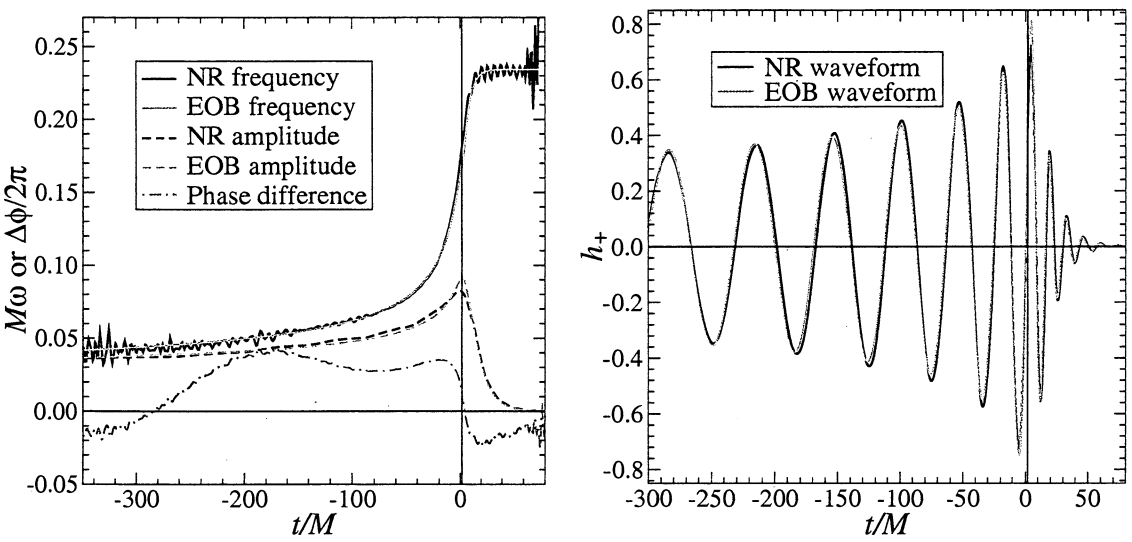

FIG. 3: Binary with mass ratio 1 : 4. In the left panel we plot the NR and EOB frequencies and amplitudes, and the phase difference between the EOB and NR h_{22}. In the right panel we compare the EOB and NR h_{22} extracted perpendicularly to the orbital plane. We maximize only on the initial phase and time of arrival.

have

$$A_{P_4^1}^{\rm p4PN}(r) = \frac{{\rm Num}(A_{P_4^1}^{\rm p4PN})}{{\rm Den}(A_{P_4^1}^{\rm p4PN})}\,, \tag{15}$$

with

$$\begin{aligned}
{\rm Num}(A_{P_4^1}^{\rm p4PN}) &= r^3\left[32-24\eta-4a_4(\eta,0)-a_5(\eta,w)\right]+r^4[a_4(\eta,0)-16+8\eta]\,, &(16)\\
{\rm Den}(A_{P_4^1}^{\rm p4PN}) &= -a_4^2(\eta,0)-8a_5(\eta,w)-8a_4(\eta,0)\eta+2a_5(\eta,w)\eta-16\eta^2+r\left[-8a_4(\eta,0)-4a_5(\eta,w)-2a_4(\eta,0)\eta-\right.\\
&\left.16\eta^2\right]+r^2\left[-4a_4(\eta,0)-2a_5(\eta,w)-16\eta\right]+r^3\left[-2a_4(\eta,0)-a_5(\eta,w)-8\eta\right]+r^4\left(-16+a_4(\eta,0)+8\eta\right)\,, &(17)
\end{aligned}$$

where

$$a_5(\eta,w) = w\,\eta\,, \tag{18}$$

and w will be determined by the comparison with numerical results. In the left panel of Fig. 1 we show how the pseudo 4PN order term w modifies the position of the EOB LSO and light-ring (the last unstable orbit for a massless particle) for several binary mass ratios. Later on we shall see that the value of w that best fits the NR results (see Sec. IV) is $w = 60$. It always guarantees the presence of a LSO and a light ring. In the right panel of Fig 1, we show the circular-orbit energy computed with the EOB Hamiltonian, and the radial potential for a massless particle, at different PN orders having fixed $w = 60$. We notice that the LSO energy ($E^{\rm EOB}_{\rm p4PN}/M = -0.0185$) and frequency ($M\omega^{\rm EOB}_{\rm p4PN} = 0.1047$) at p4PN order are closer to the corresponding values obtained using the 3PN-Taylor-expanded model for quasi-circular adiabatic orbits [29], and to the quasi-equilibrium initial-data approach [30] (see Fig. 16 and Table II in Ref. [30]). This could be a pure accident. In fact, it should be kept in mind that the LSO frequency computed from the 3PN-Taylor-expanded conservative dynamics is [29] $M\omega^{\rm T}_{\rm 3PN} \sim 0.129$ ($E^{\rm T}_{\rm 3PN}/M = -0.0193$), quite close to the formation of the common apparent horizon in the NR simulation, and quite far from the frequency ~ 0.08 at which the blurred plunge occurs [8]. What we can certainly say is that the EOB conservative dynamics at p4PN order is closer than at 3PN order to the 3PN Taylor-expanded conservative dynamics of quasi-circular adiabatic orbits [29].

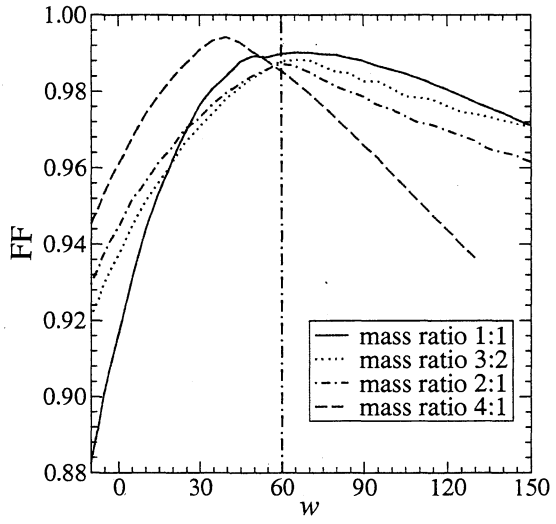

FIG. 4: For different mass ratios, we show how the FF (computed using white noise) depends on the parameter w. The vertical line refers to the value $w = 60$ which we employ in all subsequent analyses.

IV. ACCURATE EFFECTIVE-ONE-BODY WAVEFORMS FOR INSPIRAL, MERGER AND RINGDOWN

We now compare the p4PN EOB model of Sec. III with a few numerical simulations produced by the NASA-Goddard group. The numerical simulations compute directly the Weyl tensor Ψ_4, which in terms of spin-weight -2 spherical harmonics ${}_{-2}Y_{\ell m}(\theta,\varphi)$ [48] reads [see Ref. [35] for details]

$$M\,R\,\Psi_4 = \sum_{\ell m} {}_{-2}C_{\ell m}(t)\,{}_{-2}Y_{\ell m}(\theta,\varphi)\,, \tag{19}$$

being R the extraction radius. In terms of the $+$ and $\times$ GW polarizations we have

$$\Psi_4 = -(\ddot{h}_+ - i\ddot{h}_\times)\,. \tag{20}$$

Thus, we can write

$$M\,R\,C_{lm} = M\,R\int d\Omega\,{}_{-2}Y^*_{\ell m}(\theta,\varphi)\,(\ddot{h}_+ - i\ddot{h}_\times)\,. \tag{21}$$

In the adiabatic approximation ($\dot{\omega}/\omega^2 \ll 1$), we obtain

$$C_{lm} = -m^2\,\omega^2\,h_{lm}\,, \tag{22}$$

where

$$h_{lm} \equiv (h_+ - ih_\times)_{lm} = \int d\Omega\,{}_{-2}Y^*_{\ell m}(\theta,\varphi)\,(h_+ - ih_\times)\,. \tag{23}$$

We compute the EOB h_{lm} in the so-called restricted approximation, i.e., at leading order in the PN expansion. They read:

$$h^{\rm EOB}_{22} = -8\sqrt{\frac{\pi}{5}}\,\eta\,(M\,\omega)^{2/3}\,e^{-2i\,\varphi}\,, \tag{24}$$

$$h^{\rm EOB}_{21} = -\frac{8}{3}\sqrt{\frac{\pi}{5}}\,\frac{\delta m}{M}\,\eta\,(M\,\omega)\,e^{-i\,\varphi}\,, \tag{25}$$

$$h^{\rm EOB}_{32} = -\frac{8}{3}\sqrt{\frac{\pi}{7}}\,\eta\,(1-3\,\eta)\,(M\,\omega)^{4/3}\,e^{-2i\varphi}\,, \tag{26}$$

$$h^{\rm EOB}_{33} = -3\sqrt{\frac{6\pi}{7}}\,\frac{\delta m}{M}\,\eta\,(M\,\omega)\,e^{-3i\,\varphi}\,, \tag{27}$$

$$h^{\rm EOB}_{44} = -\frac{64}{9}\sqrt{\frac{\pi}{7}}\,\eta\,(1-3\eta)\,(M\,\omega)^{4/3}\,e^{-4i\,\varphi}\,, \tag{28}$$

where $\delta m = m_1 - m_2$.

The equal-mass run lasts for $\sim$ 14 GW cycles before merger. This run was published originally in Refs. [9, 35], and further studied for data-analysis purposes in Ref. [10]. The unequal-mass runs, $m_1/m_2 = 2/3, 1/2, 1/4$, last for 5, 5, and 9 GW cycles before merger. The $m_1/m_2 = 2/3, 1/2$ cases were published in References [10, 11] and the $m_1/m_2 = 1/4$ has recently been computed by the NASA-Goddard group. Adaptive mesh refinement was employed for this case as in the previous simulations, with a finest mesh resolution of $h_f = 3M/160$ used in one run and $h_f = M/64$ used in a second. Adequate convergence of the Hamiltonian and momentum constraints were found; the numerical details will be reported in a future publication. In the following analysis of the $m_1/m_2 = 1/4$ case, data from the $h_f = M/64$ run are used.

For different mass ratios, we show in Fig. 4 how the FF, obtained using white noise, depends on the parameter w. Based on this plot we decide to use in the rest of the paper $w = 60$. In Figs. 2 and 3, we plot the EOB and NR waveforms, orbital frequencies, and phase differences for the most accurate, long numerical simulations, notably the $1:1$ and $1:4$ cases. In Appendix B we show similar plots for the shorter runs $1:2$ and $2:3$.

The RD modes are attached at the time when the orbital frequency reaches its maximum and this occurs slightly before the light-ring position, $r_{\rm match}$ =??, $M\omega$ =?? ($\eta = 0.25$) and $r_{\rm match}$ =??, $M\omega$ =?? ($\eta = 0.16$). The matching is obtained by imposing the continuity of $h_{lm}(t)$ and all the higher time derivatives needed to fix the $2N$ unknown amplitudes and phases of the N RD modes [25]. Following Ref. [8], we attach the fundamental mode, and two overtones. We find that the matching-performance does not improve significantly if we add more overtones. The

η	$[M_f/M]_{\rm fromE}$	$[a_f/M_f]_{\rm from\,RD}$	$[M_f/M]_{\rm from\,fit}$	$[a_f/M_f]_{\rm from\,fit}$
0.25	0.955	0.687	0.958	0.692
0.24	0.962	0.671	0.960	0.671
0.22	0.967	0.641	0.966	0.627
0.16	0.978	0.478	0.979	0.482
0.12	...	...	0.986	0.374
0.08	...	...	0.992	0.258
0.04	...	...	0.997	0.133
0.01	...	...	0.999	0.034

TABLE I: For several values of η, we list in the second and third columns the *best*-values of M_f/M and a_f/M_f computed from the energy released and by extracting the fundamental QNM from ${}_{-2}C_{22}$, respectively. In the fourth and fifth columns we list the values obtained from the fits $M_f/M = 1 - 0.0610\,\eta - 0.4339\,\eta^2$, and $a_f/M_f = 3.441\,\eta - 2.687\,\eta^2$, respectively.

frequency and decay time of the RD modes are computed using the mass and spin of the final BH, as predicted by the numerical simulations. In fact for non-spinning binary systems, it is now possible to determine how the final-BH mass and spin depend on the mass ratio.

In Table I we list the final BH masses and spins for $\eta = 0.25, 0.24, 0.22, 0.16$, extracted from the NR simulations. The values are compatible with Ref. [47]. We also computed the final BH masses and spins to lower values of η applying a two-parameter fit to the data $\eta = 0.25, 0.24, 0.22, 0.16$. For the BH mass we use the fit function $M_f/M = 1 + a\eta + b\eta^2$, and get $a = -0.0610$ and $b = -0.4339$. Quite interestingly, the value of a is quite close to the LSO energy for a test particle in Schwarzschild, i.e., $\sqrt{8/9} - 1 \simeq -0.0572$. For the BH spin we employ the fit function $a_f/M_f = c\eta + d\eta^2$, and get $c = 3.441$ and $d = -2.687$. Again, the value of c is quite close to the LSO angular-momentum for a test particle in Schwarzschild, i.e., $\sqrt{12} \simeq 3.464$. The extrapolation to smaller values of η are consistent with the values obtained in Ref. [45] using the EOB approach.

To measure the differences between the NR and EOB waveforms we compute the *fitting factor* (FF), or ambiguity function [10, 28, 42]. The overlap $\langle h_1(t), h_2(t)\rangle$ between the waveforms $h_1(t)$ and $h_2(t)$ is defined by:

$$\langle h_1(t), h_2(t)\rangle \equiv 4\,{\rm Re}\int_0^\infty \frac{\tilde{h}_1(f)\tilde{h}_2^*(f)}{S_h(f)}df\,, \qquad (29)$$

where $\tilde{h}_i(f)$ is the Fourier transform of $h_i(t)$, and $S_h(f)$ is the detector's power spectral density (PSD). The FF is the normalized overlap between the NR waveform $h^{\rm NR}(t)$ (target) and the EOB waveform $h^{\rm EOB}(t_0,\varphi_0)$ (template) maximized *only* over the initial time t_0 and initial phase φ_0, and minimized over the initial phase φ of the target, that is

$${\rm FF} \equiv \min_{\varphi}\max_{t_0,\varphi_0} \frac{\langle h^{\rm NR}(\varphi;\lambda^i), h^{\rm EOB}(t_0,\varphi_0;\lambda^i)\rangle}{\sqrt{\langle h^{\rm NR}(\varphi;\lambda^i), h^{\rm NR}(\varphi;\lambda^i)\rangle\langle h^{\rm EOB}(t_0,\varphi_0;\lambda^i), h^{\rm EOB}(t_0,\varphi_0;\lambda^i)\rangle}}\,. \qquad (30)$$

For the detector PSD we shall consider either white noise or the LIGO noise.

In Tables II, III we list the FFs and the phase difference (in one GW cycle) between the p4PN-EOB waveform and the NR waveform, for white PSD and LIGO PSD, respectively. We consider the $l = 2, m = 2$ mode, but also other modes which are no-longer subdominant when the mass ratios decrease, as can be seen in right panel of Fig. 7. The FFs are rather high except for the $l = 4$ and $m = 4$ mode with mass-ratio 1 : 4. In this case we find that the matching procedure is not so efficient in reproducing, especially, the amplitude of the NR ringdown waveform. More studies extended to different mass ratios may shed light on this apparent anomaly.

The h_{lm} waveforms shown in Figs. 2, 3, 5 and 6, are *normalized* waveforms. In the right panel of Fig. 7, we compare the NR amplitude and EOB restricted-approximation amplitude for several l and m modes. By restricted-approximation amplitude we mean that for each l and m we restrict ourselves to the leading order term in a PN expansion. We notice, as already pointed out in Ref. [10], a non-negligible difference between the NR and EOB amplitude. We do not know what is the source of this difference. Higher-order PN corrections in the amplitude could in part nullify the difference, but due to the oscillatory behaviour of the higher PN corrections [8], it is hard to draw a robust conclusion. Moreover, there could be a systematic error in the numerical amplitude due to extraction radius or resolution issues. Although, the difference in the amplitudes has negligible

η	lm	$\langle h_{lm}^{\rm NR}, h_{lm}^{\rm EOB}\rangle$	$\Delta\varphi_{\rm GW}/(2\pi)$
0.25	22	0.9907	$\pm$0.030
0.24	22	0.9881	$\pm$0.058
0.22	22	0.9878	$\pm$0.078
0.16	22	0.9925	$\pm$0.035
0.16	33	0.9860	$\pm$0.055
0.16	44	0.9436	$\pm$0.065

TABLE II: For several mass configurations, we list the FF obtained using white noise and maximizing only on the time of arrival and initial phase, and the phase difference in one GW cycles.

(m_1+m_2)	lm	$\langle h_{lm}^{\rm NR}, h_{lm}^{\rm EOB}\rangle$	$\Delta\varphi_{\rm GW}/(2\pi)$
$(15+15)M_\odot$	22	0.9975	$\pm$0.043
$(50+50)M_\odot$	22	0.9817	$\pm$0.043
$(20+30)M_\odot$	22	0.9897	$\pm$0.065
$(20+40)M_\odot$	22	0.9889	$\pm$0.068
$(10+40)M_\odot$	22	0.9961	$\pm$0.035
$(10+40)M_\odot$	33	0.9911	$\pm$0.055
$(10+40)M_\odot$	44	0.9720	$\pm$0.075
$(20+80)M_\odot$	22	0.9965	$\pm$0.035
$(20+80)M_\odot$	33	0.9873	$\pm$0.055
$(20+80)M_\odot$	44	0.9548	$\pm$0.065

TABLE III: For several mass configurations, we list the FFs obtained using LIGO PSD and maximizing only on the time of arrival and initial phase, and the phase difference in one GW cycles.

effects on the fitting-factors [10], it needs to be sorted out.

V. CONCLUSIONS

In this paper we started exploiting the flexibility of the EOB approach to build accurate waveforms for non-spinning binary BHs. We obtained phase differences between the EOB and NR waveforms of less than 8% in a GW cycle, for mass ratios $\eta = 0.25, 0.24, 0.22$ and $\eta = 0.16$. The p4PN EOB model can be used to predict waveforms for values of *eta* < 0.16, that can be tested against numerical simulations when accurate, long waveforms will become available.

The improved EOB model is obtained by simply adding a p4PN order constant coefficient ($w = 60$) in the EOB radial potential $A(r)$ and Padeing the latter to guarantee the presence of the LSO and the light-ring. This modification provides a better agreement between the EOB and NR GW frequency during the transition inspiral(-plunge) to ringdown. The complete waveform is then built by attaching three QNMs at the peak of the EOB GW frequency. The QNM frequency and decay time are fixed by the final BH mass and spin, which can be predicted by extrapolating sparse NR results, either through a fit (see Table I) or within the EOB model itself [45].

We point out, as already done in Ref. [10], that there exists a non-negligible difference in the amplitude of the PN (EOB or Taylor-expanded-PN) and NR waveforms, whose origin has not yet been accounted for. It might be due to higher-order PN corrections in the amplitude or numerical systematic errors.

Using white PSD, we found FFs $\gtrsim 0.98$, except for the $l = 4$ and $m = 4$ mode of mass ratio 1 : 4 which has FF $= 0.94$ (see Table II). At present time, we do not know what is the reason of this anamaly. It could be due to a failure of the matching procedure due to the presence of other QNMs. All FFs are achieved by maximizing *only* on the initial phase and time of arrival of the template (and by minimizing on the initial phase of the target). Since we do *not* maximize on the binary's intrinsic parameters, that is the BH masses, the p4PN-EOB model can be used for parameter estimation. Depending on the binary total mass and mass ratios, FFs $\gtrsim$0.98 are obtained with LIGO PSD (see Table III), except for the $l = 4, m = 4$ mode, which has FF $= 0.95$–0.97, depending on the total binary mass.

When maximizing on the binary masses, the p4PN-EOB waveform will have extremely high matching performances (FF $\gtrsim 0.99$) and can be used for coherent detection of non-spinning binary BHs. In the future we plan to extend this analysis to spinning, precessing binary systems, using improved versions of the EOB model with spin [24, 27]. Once a complete analytic model for inspiral-merger-ringdown is worked out, we shall employ the detection schemes proposed in Refs. [41, 43] to deal with intrinsic and extrinsic parameters in the presence of spins, and provide accurate templates to be used by ground-based and space-based detectors.

Acknowledgments

A.B. and Y.P. acknowledge support from NSF grant PHY-0603762, and A.B. also acknowledges support from the Alfred P Sloan Foundation. The work at Goddard was supported in part by NASA grants O5-BEFS-05-0044 and 06-BEFS06-19. B.K. was supported by the NASA Postdoctoral Program at the Oak Ridge Associated Universities. S.T.M. was supported in part by the Leon A. Herreid Graduate Fellowship.

APPENDIX A: COMPARISON OF MULTIPOLES WITH $l \neq 2$ AND $m \neq 2$

Here we discuss how the p4PN-EOB waveforms having $l \neq 2$ and $m \neq 2$ compare with the NR ones. We consider the dominant modes, that is $l = 3, m = 3$, $l = 4, m = 4$, $l = 3, m = 2$ and $l = 2, m = 1$, and restrict the analysis to the case with mass ratio 1 : 4.

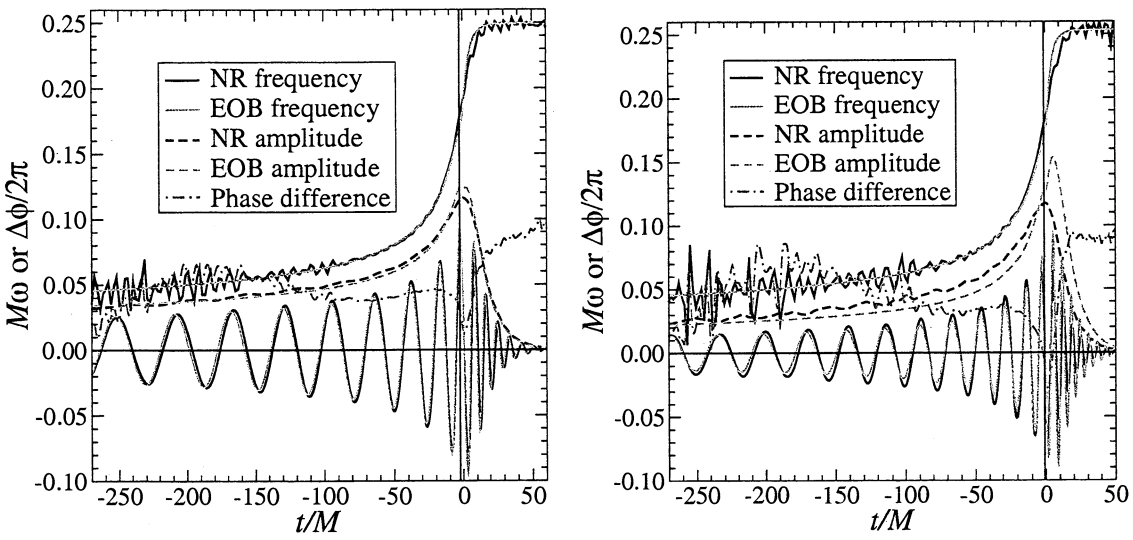

FIG. 5: Binary with mass ratio 1 : 4. In the left (right) panel we plot the h_{33} (h_{44}) mode. We maximize only on the initial phase and time of arrival.

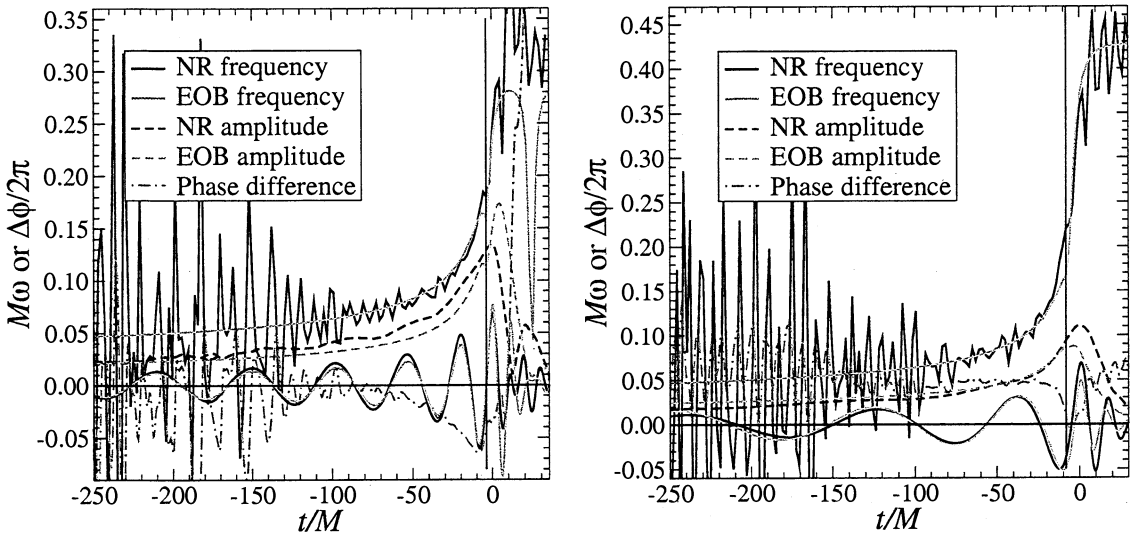

FIG. 6: Binary with mass ratio 1 : 4. In the left (right) panel we plot the h_{32} (h_{21}) mode. We maximize only on the initial phase and time of arrival.

APPENDIX B: COMPARISON WITH BINARIES OF MASS RATIO 1 : 2 AND 2 : 3

In this appendix we show how the p4PN-EOB model performs for mass ratios 1 : 2 and 2 : 3. In these cases the waveforms are much shorter, and the eccentricity during the inspiral case is more pronounced.

[1] A. Abramovici et al., Science **256**, 325 (1992); http://www.ligo.caltech.edu.
[2] H. Lück et al., Class. Quant. Grav. **14**, 1471 (1997); http://www.geo600.uni-hannover.de.
[3] M. Ando et al., Phys. Rev. Lett. **86**, 3950 (2001); http://tamago.mtk.nao.ac.jp.
[4] B. Caron et al., Class. Quant. Grav. **14**, 1461 (1997); http://www.virgo.infn.it.
[5] http://www.lisa-science.org/resources/talks-articles/science/lisa_science_case.pdf

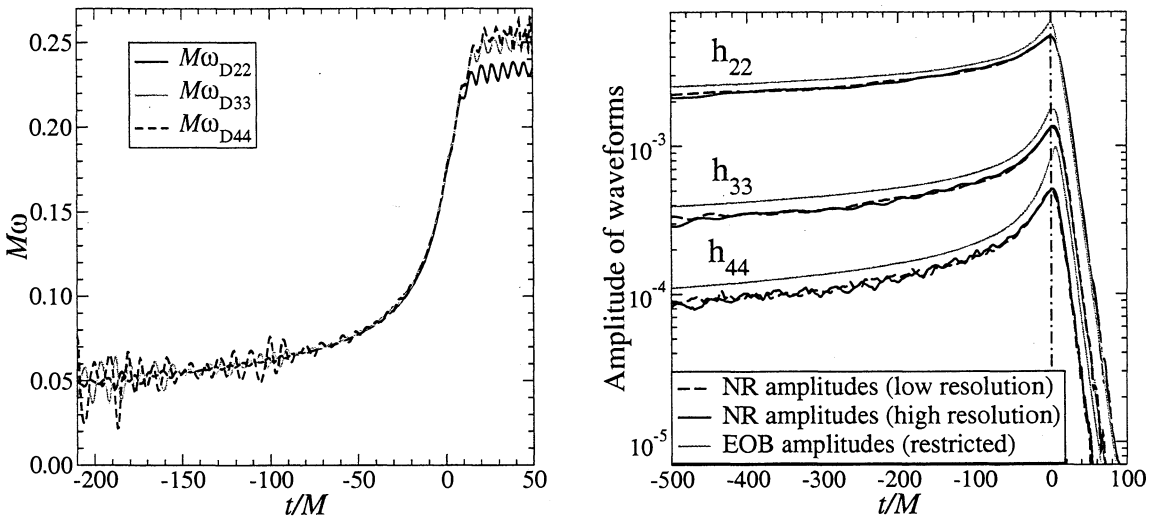

FIG. 7: Binary with mass ratio 1 : 4. In the left panel we plot the dominant frequencies for several l and m modes. Generalizing Eq. (XXX) in Ref. [8], we define $\omega_{Dlm} = -(1/m)\,\mathrm{Im}(\dot{C}_{lm}/C_{lm})$ [11]. In the right panel we compare the NR amplitude and EOB restricted-approximation amplitude for several l and m modes. By restricted-approximation amplitude we mean that for each l and m we restrict ourselves to the leading order term.

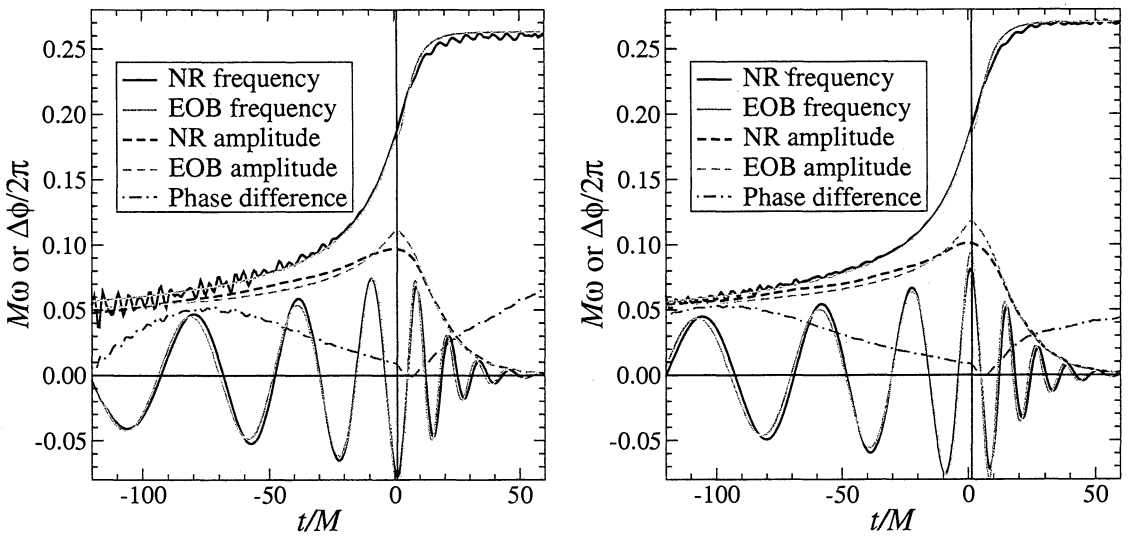

FIG. 8: In the left (right) panel we plot the NR and EOB frequencies and amplitudes, and the phase difference between the EOB and NR h_{22} for a binary with mass ratio 1 : 2 (2 : 3). We maximize only on the initial phase and time of arrival.

[6] L.S. Finn, Phys. Rev. D **46**, 5236 (1992); L. S. Finn and D.F. Chernoff, Phys. Rev. D **47**, 2198 (1993); É.E. Flanagan and S.A. Hughes, Phys. Rev. D **57**, 4535 (1998).

[7] See, e.g., L. Blanchet, Living Rev. Rel. **5**, 3 (2002).

[8] A. Buonanno, G. Cook, and F. Pretorius, in press on Phys. Rev. D [gr-qc/0610122].

[9] J. Baker, J. van Meter, S. McWilliams, J. Centrella, and B. Kelly (2006), [gr-qc/0612024].

[10] Y. Pan, A. Buonanno, J.G. Baker, J. Centrella, B. Kelly, and S.T. McWilliams, F. Pretorius, and J. R. van Meter, *Data-analysis driven comparison of analytic and numerical coalescing binary waveforms: non-spinning case*, submitted to Phys. Rev. D [gr-qc/07041964].

[11] J. Schnittman, A. Buonanno, J. R. van Meter, J.G. Baker, W.D. Boggs, J. Centrella, B. Kelly, and S.T. McWilliams, *Anatomy of the binary black hole recoil: a multipolar analysis*, (in preparation).

[12] F. Pretorius, Phys. Rev. Lett. **95**, 121101 (2005); M. Campanelli, C.O. Lousto, P. Marronetti, and Y. Zlochower, Phys. Rev. Lett. **96**, 111101 (2006); J. Baker, J. Centrella, D. Choi, M. Koppitz, and J. van Meter, Phys. Rev. Lett. **96**, 111102 (2006).

[13] M. Campanelli, C.O. Lousto, and Y. Zlochower, Phys. Rev. D **74**, 041501 (2006); ibid. D **74**, 084023 (2006); U. Sperhake, gr-qc/0606079; J. González, U. Sperhake, B. Brügmann, M. Hannam, and S. Husa, Phys. Rev. Lett. **98**, 091101 (2007); B. Szilagyi, D. Pollney, L. Rezzolla, J. Thornburg and J. Winicour, 0612150; F. Pretorius and

D. Khurana, gr-qc/0702084.
[14] P. Jaranowski and G. Schafer, Phys. Rev. D **57**, 7274 (1998) [Erratum-ibid. D **63**, 029902 (2001)].
[15] T. Damour, P. Jaranowski and G. Schafer, Phys. Lett. B **513**, 147 (2001).
[16] T. Damour, P. Jaranowski and G. Schafer, Phys. Rev. D **62**, 021501 (2000) [Erratum-ibid. D **63**, 029903 (2001)].
[17] L. Blanchet, and G. Faye, Phys. Rev. D **63**, 062005 (2001); V. C. de Andrade, L. Blanchet, and G Faye, Class. Quant. Grav. **18**, 753 (2001); L. Blanchet, G. Faye, B.R. Iyer, and B. Joguet, Phys. Rev. D **65**, 061501(R) (2002); Erratum-ibid D **71**, 129902 (2005); L. Blanchet, and B.R. Iyer, Class. Quant. Grav. **20**, 755 (2003); Erratum-ibid D **71**, 129902 (2005); L. Blanchet, T. Damour, G. Esposito-Farese, and B.R. Iyer, Phys. Rev. Lett. **93**, 091101 (2004).
[18] L. Kidder, C. Will, and A. Wiseman, Phys. Rev. D **47**, 4183 (1993); L. Kidder, Phys. Rev. D **52**, 821 (1995); B. Owen, H. Tagoshi, and Ohashi, Phys. Rev. D **57**, 6168 (1998); H. Tagoshi, Ohashi, and B. Owen, Phys. Rev. D **63**, 044006 (2001); L. Blanchet, A. Buonanno, and G. Faye, Phys. Rev. D **74**, 104034 (2006); G. Faye, L. Blanchet, and A. Buonanno, Phys. Rev. D **74**, 104033 (2006).
[19] L. E. Kidder, C. M. Will and A. G. Wiseman, Phys. Rev. D **47**, 3281 (1993).
[20] N. Wex and G. Schafer, Class. Quantum Grav. **10**, 2729 (1993).
[21] A. Buonanno, and T. Damour, Phys. Rev. D **59**, 084006 (1999).
[22] E. Brézin, C. Itzykson and J. Zinn-Justin, Phys. Rev. D **1**, 2349 (1970).
[23] T. Damour, P. Jaranowski, and G. Schäfer, Phys. Rev. D **62**, 084011 (2000).
[24] T. Damour, Phys. Rev. D **64**, 124013 (2001).
[25] A. Buonanno, and T. Damour, Phys. Rev. D **62**, 064015 (2000).
[26] A. Buonanno, and T. Damour, Proceedings of IX$^{\rm th}$ Marcel Grossmann Meeting (Rome, July 2000), [gr-qc/0011052].
[27] A. Buonanno, Y. Chen, and T. Damour, Phys. Rev. D **74**, 104005 (2006).
[28] T. Damour, B.R. Iyer, and B.S. Sathyaprakash, Phys. Rev. D **67**, 064028 (2003).
[29] L. Blanchet, Phys. Rev. D **65**, 124009 (2002).
[30] G. B. Cook, and H. P. Pfeiffer, Phys. Rev. D **70**, 104016 (2004); M. Caudill, G.B. Cook, J.D. Grigsby, and H. Pfeiffer, Phys. Rev. D **74**, 064011 (2006).
[31] T. Damour, B. Iyer, P. Jaranowski, and B. Sathyaprakash, Phys. Rev. D **67**, 064028 (2003).
[32] T. Damour, B. Iyer, and B. Sathyaprakash, Phys. Rev. D **63**, 044023 (2001); ibid. D **66**, 027502 (2002).
[33] T. Damour, E. Gourgoulhon, and P. Grandclément, Phys. Rev. D **66**, 024007 (2002).
[34] E. Gourgoulhon, P. Grandclément, and S. Bonazzola, Phys. Rev. D **65**, 044020 (2002); P. Grandclément, E. Gourgoulhon, and S. Bonazzola, Phys. Rev. D **65**, 044021 (2002).
[35] J. Baker, S. McWilliams, J. van Meter, J. Centrella, D. Choi, B. Kelly, and M. Koppitz (2006), [gr-qc/0612117].
[36] B. Abbott et al. (LIGO Scientific Collaboration), Phys. Rev.D **72**, 082001 (2005).
[37] B. Abbott et al. (LIGO Scientific Collaboration), Phys. Rev. D **73**, 062001 (2006).
[38] E. Berti, V. Cardoso, and C. Will, Phys. Rev. D **73**, 064030 (2006).
[39] L. Blanchet, Living Rev. Rel. 9 (2006) 4.
[40] T. Damour, B.R. Iyer, and B.S. Sathyaprakash, Phys. Rev. D **57**, 885 (1998).
[41] A. Buonanno, Y. Chen, and M. Vallisneri, Phys. Rev. D **67**, 104025 (2003); Erratum-ibid. D **74**, 029904 (2006).
[42] A. Buonanno, Y. Chen, and M. Vallisneri, Phys. Rev. D **67**, 024016 (2003); Erratum-ibid. D **74**, 029903 (2006).
[43] Y. Pan, A. Buonanno, Y. Chen, and M. Vallisneri, Phys. Rev. D **69**, 104017 (2004).
[44] A. Nagar, T. Damour, and A. Tartaglia, [gr-qc/0612096] T. Damour, and A. Nagar, Proceedings of XI$^{\rm th}$ Marcel Grossmann Meeting (Berlin, July 2006), [gr-qc/0612151].
[45] T. Damour and A. Nagar, [gr-qc/07043550].
[46] T. Damour and A. Nagar, [gr-qc/07052519].
[47] See J. González et al. in Ref. [13].
[48] Y. Wiaux, L. Jacques, P. Vandergheynst, [astro-ph/0508514].
[49] C.V. Vishveshwara, Nature **227**, 936 (1970); B. Schutz and C.M. Will, Astrophys. J. **291**, 33 (1985); S. Chandrasekhar and S. Detweiler, Proc. R. Soc. Lond. A **344**, (1975) 441.
[50] W. Press, Astrophys J. Letters **170**, L105 (1971).
[51] M. Davis, R. Ruffini, W.H. Press, and R.H. Price, Phys. Rev. Lett. **27**, 1466 (1971); M. Davis, R. Ruffini, and J. Tiomno, Phys. Rev. D **5**, 2932 (1972).
[52] R.H. Price and J. Pullin, Phys. Rev. Lett. **72**, 3297 (1994); R.J. Gleiser, C.O. Nicasio, R. Price, and J. Pullin, Class. Quant. Grav. **13**, L117 (1996); Phys. Rev. Lett. **77**, 4483 (1996); P. Anninos, D. Hobill, E. Seidel, L. Smarr, and W.M. Suen, Phys. Rev. Lett. **71**, 2851 (1993); Z. Andrade and R. H. Price, Phys.Rev.D **56**, 6336 (1997).
[53] T. Damour and A. Gopakumar, Phys. Rev. D **73**, 124006 (2006).
[54] When using the EOB real Hamiltonian we should in principle consider the (generalized) canonical transformation between the real and effective variables which is explicitly given as a PN expansion in Refs. [21, 23]. However, since the Hamilton equations are valid in any canonical coordinate system, when we evolve the EOB dynamics we write the Hamilton equations in terms of the effective variables. When comparing to NR results, there might be some differences in the time variable, though.